Multi-feature localization of epileptic foci from interictal, intracranial EEG

Jan Cimbalnik, PhD[a,b,*], **Petr Klimes, PhD**[a,b,c,*], **Vladimir Sladky, M.Sc**[a,b], **Petr Nejedly, B.Sc.**[a,b,c], **Pavel Jurak, PhD**[c], **Martin Pail, PhD**[d], **Robert Roman, PhD**[e], **Pavel Daniel, M.Sc**[d], **Hari Guragain, PhD**[b], **Benjamin Brinkmann, PhD**[b,f], **Milan Brazdil, MD, PhD**[d,e], **Greg Worrell, MD, PhD**[b,f]

[a]International Clinical Research Center, St. Anne's University Hospital, Brno, Czech Republic

[b]Mayo Systems Electrophysiology Laboratory, Department of Neurology, Mayo Clinic, 200 First St SW, Rochester MN, 55905, USA

[c]Institute of Scientific Instruments, The Czech Academy of Sciences, Brno, Czech Republic

[d]Brno Epilepsy Center, Department of Neurology, St. Anne's University Hospital and Faculty of Medicine, Masaryk University, Brno, Czech Republic

[e]Behavioral and Social Neuroscience Research Group, CEITEC – Central European Institute of Technology, Masaryk University, Brno, Czech Republic

[f]Department of Physiology and Biomedical Engineering, Mayo Clinic, 200 First St SW, Rochester MN, 55905, USA

Abstract

Objective—In drug-resistant epilepsy, 40–50% of patients suffer from seizure recurrence. To achieve seizure freedom without side effects, accurate localization of the epileptogenic tissue is

Correspondence to: Jan Cimbalnik, PhD, Department of Biomedical Engineering; International Clinical Research Center (FNUSA-ICRC), St. Anne's University Hospital in Brno, Peka ská 53, Brno, 656 91, Czech Republic, Tel.: +420 543 185 584, jan.cimbalnik@fnusa.cz.
*Co-first authors for this study.

Conflicts of Interest

Dr. Cimbalnik reports In addition, Dr. Cimbalnik has a patent SEIZURE ONSET ZONE LOCALIZATION pending.

Dr. Klimes has nothing to disclose.

Sladky has nothing to disclose.

Nejedly has nothing to disclose.

Dr. Jurak has nothing to disclose.

Dr. Pail has nothing to disclose.

Dr. Roman has nothing to disclose.

Mr. Daniel has nothing to disclose.

Dr. Guragain has nothing to disclose.

Dr. Brinkmann reports non-financial support from Medtronic, Inc., outside the submitted work; In addition, Dr. Brinkmann has a patent MULTISCALE BRAIN ELECTRODE DEVICES issued.

Dr. Brazdil has nothing to disclose.

Dr. Worrell reports other from NeuroOne Inc, outside the submitted work; In addition, Dr. Worrell has a patent Localization of epileptogenic brain pending.

crucial before its resection. We investigate an automated, fast, objective mapping process that uses only interictal data.

Methods—We propose a novel approach based on multiple iEEG features, which are used to train a support vector machine (SVM) model for classification of iEEG electrodes as normal or pathologic using 30 minutes of inter-ictal recording.

Results—The tissue under the iEEG electrodes, classified as epileptogenic, was removed in 17/18 excellent outcome patients and was not entirely resected in 8/10 poor outcome patients. The overall best result was achieved in a subset of 9 excellent outcome patients with the area under the receiver operating curve = 0.952.

Conclusion—SVM models combining multiple iEEG features show better performance than algorithms using single iEEG marker. Multiple iEEG and connectivity features in presurgical evaluation could improve epileptogenic tissue localization, which may improve surgical outcome and minimize risk of side effects.

Keywords

drug resistant epilepsy; epileptogenic zone localization; multi-feature approach; high frequency oscillations; connectivity; machine learning

---

1. Introduction

Epilepsy is one of the most prevalent neurological diseases (Leonardi and Ustun, 2002). While roughly two-thirds of patients with epilepsy are successfully managed with anti-seizure drugs (ASDs), the remaining patients continue to have seizures and may be candidates for surgical treatment options (Wiebe et al., 2001).

Precise localization of the focal region generating a patient's seizures is required for surgical resection, the most effective (Téllez-Zenteno et al., 2010) and commonly performed treatment (Kelly and Chung, 2011), and to guide implantation of electrodes for therapeutic brain stimulation (Fisher and Velasco, 2014; Bergey et al., 2015). Accurate localization of epileptogenic tissue is critical for achieving optimal outcomes and minimizing risk of side effects.

Currently, the clinical gold-standard for localization of epileptogenic tissue is obtained by recording spontaneous seizures with intracranial EEG (iEEG). This requires days to weeks of recording and can be associated with patient discomfort and risk, (Van Gompel et al., 2008). The iEEG is used in combination with other modalities to ensure concordance of the multi-modal information but when considering all types of focal epilepsy the seizure-free outcome is achieved in only approximately 50% of patients (Téllez-Zenteno et al., 2010).

The visual analysis of the massive iEEG datasets is time consuming and subject to observer biases. Naturally, this has led to many attempts for automated localization of epileptogenic tissue from interictal iEEG recordings, which would significantly speed up the pre-surgical evaluation process. Many of these seizure-independent methods use high-frequency EEG power or rates of high-frequency oscillations (HFO) (Bragin et al., 2002; Jacobs et al., 2008;

Worrell et al., 2008; Cimbalnik et al., 2016). These methods show promise for pathological tissue localization, and have been shown successful in $\frac{2}{3}$ of the patients (Cimbálník et al., 2018; Jacobs et al., 2018). The reason for the failures might be caused by false positive detections (Bénar et al., 2010) or by the fact that physiological HFOs (Kucewicz et al., 2014; Brázdil et al., 2015) are challenging to distinguish from pathological HFOs (Matsumoto et al., 2013; Cimbalnik et al., 2018).

Recently, functional connectivity was described as a new biomarker of the epileptogenic zone, i.e. the tissue that must be resected or disconnected for seizure freedom (Lüders and Comair, 2001). During the inter-ictal period, different connectivity patterns have been reported in a normal epileptic brain compared to the seizure onset zone (SOZ) (Bettus et al., 2008; Dauwels et al., 2009; Warren et al., 2010), which is also functionally isolated from surrounding healthy tissue (Warren et al., 2010; Klimes et al., 2016). Altered connectivity pattern in the epileptic brain has also been used to predict surgery outcome (Antony et al., 2013).

Despite the promise of seizure-independent biomarkers, no single marker has been consistently shown to be effective for all patients (Cimbalnik et al., 2018; Jacobs et al., 2018). Electrophysiological activity of the brain is not consistent across time (Pearce et al., 2013; Gliske et al., 2018) and is affected by different states of vigilance (Gross and Gotman, 1999; Staba et al., 2002; Kremen et al., 2017). Therefore, utilizing the HFO rate, or connectivity as a stand-alone biomarker is unlikely to be successful in all cases (Khadjevand et al., 2017; Cimbalnik et al., 2018; Jacobs et al., 2018). Combination of multiple features might provide a more robust estimation (Gnatkovsky et al., 2014; Varatharajah et al., 2018).

Here we explore the utility of combining different information represented by multiple iEEG biomarkers. A previous study by Varatharajah et al. (Varatharajah et al., 2018) used a combination of univariate features (HFO rate and phase-amplitude coupling) for SOZ localization (Varatharajah et al., 2018). We investigated a combination of univariate and bivariate iEEG features given they are likely to carry different information. These features are used to train the Support Vector Machine (SVM) model which is used to identify electrodes with the highest probability of being in the epileptogenic region.

2. Methods

To promote transparency and ensure reproducibility of our results, the SVM code and feature data are available online (https://github.com/ICRC-BME/machine_learn_module).

2.1. Patients

All patients underwent intracranial depth and subdural electrode implantation as part of their evaluation for epilepsy surgery when non-invasive studies could not adequately localize the seizure onset zone. All patients recorded in the Brno Epilepsy Center or Mayo Clinic between years 2011 and 2016 were selected for this study. Patients without implanted white matter, electrode coordinates, SOZ information or with poor recording quality were omitted from the cohort. The final cohort of patients, who participated in the study, consisted of 43 patients from Brno Epilepsy Center and 34 from Mayo Clinic (Supplementary Table 1).

Since we used three different targets for classification (1. SOZ contacts, 2. resected contacts, 3. SOZ overlapped with resected contacts), the final cohort was further divided into three subgroups. For SOZ target all patients were included. For resected contacts target only patients with information about surgical outcome and resected area were included resulting in a subgroup of 30 patients (9 good and 7 bad outcome patients in Brno Epilepsy Center, 9 good and 5 bad outcome patients in Mayo Clinic). For SOZ overlapped with resected contacts target the subgroup consisted of 28 patients (9 good and 5 bad outcome patients in Brno Epilepsy Center, 9 good and 5 bad outcome patients in Mayo Clinic). The information about the resected area was available only in 30 patients (16 in Brno dataset, 14 in Mayo dataset) mostly due to poor quality of imaging data (slices > 2 mm) or implantation of vagus nerve stimulator. The numbers of patients in each group are available in Table 1.

The study was approved by the Brno Epilepsy Center - St. Anne's University Hospital Research Ethics Committee and the Mayo Clinic Institutional Review Board. All patients provided informed consent.

2.2. Intracranial EEG recordings

2.2.1. Brno Epilepsy Center, St. Anne's University Hospital—43 patients implanted with standard intracranial depth electrodes (5, 10 and 15 contact semi-flexible multi-contact platinum electrodes DIXI (DIXI MEDICAL; CHAUDEFONTAINE, FRANCE) or ALCIS(ALCIS, Besançon, France), contact surface area 5.02 mm^2 and inter-contact distance 1.5 mm). All iEEG was acquired with a common reference, an average signal from all iEEG channels. The iEEG was recorded with a sampling frequency of 25 kHz. The data was down-sampled to 5 kHz for further processing. 30 minutes of relaxed awake activity was selected for the analysis. Anatomical localization of electrodes was achieved using post-implant MRI co-registered to the patient's pre-implant MRI.

2.2.2. Electrophysiology Laboratory, Mayo Clinic—34 patients, all implanted with intracranial depth electrodes (AD-Tech Medical Inc, Racine, WI, 4 and 8 contact clinical depth electrodes with Platinum/Iridium clinical macro-electrode contacts, contact surface area 9.4 mm^2 and inter-contact distance 10 mm) and subdural grids and strips (4.0 mm diameter Platinum/Iridium discs (2.3 mm diameter exposed) with 10 mm inter-contact distance). All intracranial EEG was acquired with a stainless steel suture as a common reference placed in the vertex region of the scalp midline between the international 10–20 Cz and Fz electrode positions. The iEEG was recorded with a sampling frequency of 32 kHz and down-sampled to 5 kHz, with a 1kHz Bartlett-Hanning window low-pass filter. 30 minutes from 1 AM to 1:30 AM of the patient's first night at ICU was selected for analysis. The location of electrodes was determined from post-implant CT data co-registered to the patient's pre-implant MRI using normalized mutual information (SPM8). Electrode coordinates were then automatically labeled by SPM Anatomy toolbox, with an estimated accuracy of 5 mm (Tzourio-Mazoyer et al., 2002).

2.3. EEG signal pre-processing

A visual inspection and automated detection based on convolutional neural networks was used to detect noise, technical artifacts, muscle and movement artifacts (Nejedly et al.,

2018). Bad data segments or whole EEG channels were omitted from further analysis. To remove scalp reference and suppress far-field potentials caused predominantly by volume conduction a reference signal was calculated and subtracted from each iEEG signal. The reference signal was calculated as an average signal from iEEG electrodes placed in the white matter.

2.4. Identification of seizure onset zone

The seizure onset electrodes and time of seizures were determined from the clinical report and verified independently by identifying the electrodes with the earliest iEEG seizure discharge. Seizure onset times and location were determined by visual identification of a clear electrographic seizure discharge, followed by a look back in the iEEG recordings for the earliest electroencephalographic change contiguously associated with the seizure.

2.5. Identification of resected tissue

Post-resection MRI was used to identify areas of the brain that were surgically removed. The electrodes localized within the resected areas were marked.

2.6. Surgical Outcomes

Surgical outcomes were classified according to the International League Against Epilepsy (ILAE) classification system at Mayo Clinic and Engel Surgical Outcome Scales at Brno. ILAE Class-1 and Engel class IA were considered good outcome.

2.7. Calculated features

The EEG features were computed in three distinct groups: 1) HFO features - computed from detections of oscillatory events in the iEEG signal, 2) univariate features - computed on iEEG signal from individual iEEG channel on a depth electrode, 3) bivariate features - computed between two iEEG signals from two adjacent iEEG channels on a depth electrode. In grid contacts the adjacent channels were determined along the longitudinal axis of the grid. HFOs and oscillatory events below HFO frequency bands (< 80 Hz) were detected in 10 sec, non-overlapping statistical windows. Mean rate per channel was then calculated for the whole length of recording. Univariate and bivariate EEG features were calculated in 1 sec non-overlapping windows. The mean feature value of all 1 sec windows was calculated for each channel or channel pair. To obtain one value per contact for bivariate features only the higher of the two mean feature values was selected. All features were calculated in 9 different frequency bands (1–4 Hz, 4–8 Hz, 8–12 Hz, 12–20 Hz, 20–45 Hz, 55–80 Hz, 80–250 Hz, 250–600 Hz, 600–1000 Hz), except frequency- and phase-amplitude coupling, which were calculated for fixed pair of frequencies only. The data were filtered using 2nd order IIR bandpass Butterworth filters. All features were normalized by z-score normalization before SVM model training and testing.

2.7.1. HFO rate—Various HFO detectors have been described in the literature, and direct comparison of detectors remains challenging (Roehri et al., 2017). In this study, two different HFO detectors were used: **1)** The line-length detector (Gardner et al., 2007) which is sensitive to any increase in band power but its specificity is low, especially with regard to

false ripples created by sharply contoured transients. This detector was run in all frequency bands. The detection thresholds were set to 3 standard deviations of the line-length metric above the mean and the duration threshold was set to a minimum of 5 oscillations. **2)** The CS detector has been proven to successfully eliminate false ripples produced by band pass filtering of sharp transients (Cimbálník et al., 2018). The threshold for the detection was set to 0.1 and the duration threshold set to a minimum of 5 oscillations. This detector was run in parallel with the LL detector. Since the CS detector provides detections with determined frequency, the HFO rate in individual frequency bands was determined ad-hoc by the sum of detections that fell within the frequency cut-offs of each frequency band. The resulting HFO rates of the LL and CS detectors were treated as separate features.

2.7.2.   Power in band (univariate feature)—Increased Local Field Potential (LFP) amplitude is primarily caused by synchronized activity of local neuronal synapses and provides information about electrophysiological activity of measured region (Katzner et al., 2009). Relative power in band (PB) for each iEEG channel was calculated as $PB = \ <X_t^2>/<X_{t\_raw}2>$, where $<>$ stands for mean, X_t for the signal in selected frequency band and $X_{t\_raw}2$ for the non-filtered signal.

2.7.3.   Frequency amplitude coupling (univariate feature)—Frequency amplitude coupling reflects how the signal amplitude is modulated by a particular frequency band. Unlike other features, this method used fixed pair of frequency bands: lower (1–30 Hz) for time signal and higher (65–180 Hz) for signal envelope (Varatharajah et al., 2018). Frequency amplitude coupling (FAC) was calculated as $FAC=[cov(|x_H|,x_t)/std(|x_H|) \cdot std(x_t)]$, where x_t is the time signal filtered in lower frequency band, x_H is the Hilbert transformation of the time signal *filtered in higher frequency band*, *cov* stands for the covariance and *std* for the standard deviation. The value of FAC varies in interval $<-1,1>$. *FAC=1* indicates perfect dependence between frequency and amplitude, *FAC=−1* indicates opposite dependence, and *FAC=0* indicates no dependence.

2.7.4.   Phase amplitude coupling (univariate feature)—Phase amplitude coupling reflects how the signal amplitude is modulated by its instantaneous phase of particular frequency band. Similarly to FAC, this method used fixed pair of frequency bands: lower (1–30 Hz) for instantaneous phase and higher (65–180 Hz) for signal envelope (Varatharajah et al., 2018). Instantaneous phase was calculated as $\Phi_t=arctan(x_H/x_t)$, where x_H is the Hilbert transformation of the time signal x_t, which was previously filtered in lower frequency band. Phase amplitude coupling (PAC) was then calculated as $PAC=[cov(|X_H|,\Phi_t)/std(|X_H|) \cdot std(\Phi_t)]$, where X_H is the Hilbert transformation of the time signal, which was previously filtered in higher frequency band, *cov* stands for the covariance and *std* for the standard deviation. The value of PAC varies in interval $<-1,1>$. *PAC=1* indicates perfect dependence between phase and amplitude, *PAC=−1* indicates opposite dependence, and *PAC=0* indicates no dependence.

2.7.5.   Power spectral entropy (univariate feature)—In general, information entropy is defined as the average amount of information in observed data. In signal

processing, entropy reflects a randomness and spectral richness in continuous time-series. Power spectral entropy (PSE) was calculated as $PSE=-sum[ps \cdot log_2(ps)]$, where ps is a fraction of particular examples in the dataset, in this case normalized spectral power density obtained by Fourier transformation.

2.7.6.   Relative entropy (bivariate feature)—To evaluate the randomness and spectral richness between two time-series, the Kullback-Leibler divergence, i.e. relative entropy (REN), was calculated. REN is a measure of how entropy of one signal diverges from a second, expected one. The value of REN varies in interval <0,+Inf>. $REN=0$ indicates the equality of statistical distributions of two signals, while $REN>0$ indicates that the two signals are carrying different information. REN was calculated between adjacent iEEG channels X, Y as $REN=sum[pX \cdot log(pX/pY)]$, where pX is a probability distribution of investigated signal and pY is a probability distribution of expected signal. Because of asymmetrical properties of REN, REN(X, Y) is not equal to REN(Y, X). REN was calculated in two steps for both directions (both distributions from channel pair were used as expected distributions). The maximum value of REN was then considered as the final result, regardless of direction.

2.7.7.   Correlation (bivariate feature)—The linear correlation (LC) varies in interval < −1,1> and reflects shape similarities between two signals. $LC=1$ indicates perfect conformity between two signals, $LC=−1$ indicates opposite signals and $LC=0$ indicates two different signals. LC was calculated by Pearson's correlation coefficient as: $LC_{X,Y}=[cov(X_t, Y_t)/std(X_t) \cdot std(Y_t)]$, where X_t, Y_t are the two evaluated signals, cov is the covariance and std is the standard deviation.

2.7.8.   Correlation with time-lag (bivariate feature)—The linear correlation between all adjacent iEEG channels was calculated in 1 second non-overlapping intervals with a time-lag. Maximum time-lag was equal to $f_{max}/2$ of selected frequency band. Lagged linear correlation (LLC) for each time-lag k was calculated by Pearson's correlation coefficient as: $LLC_{X(k), Y(k)}=[cov(X_{t(k)}, Y_{t(k)})/std(X_{t(k)}) \cdot std(Y_{t(k)})]$, where X_t, Y_t are the two evaluated signals, cov is the covariance and std is the standard deviation. The maximum value of correlation was stored with its time-lag value. Time-lag of maximum LLC value was evaluated as a separate feature.

2.7.9.   Phase lag index (bivariate feature)—Phase lag index (PLI) represents evaluation of statistical interdependencies between time series, which is supposed to be less influenced by the common sources (Stam et al., 2007). PLI calculation is based on the phase synchronization between two signals with constant, nonzero phase lag, which is most likely not caused by volume conduction from a single strong source. Phase lag index was calculated as $PLI = |< sign[\Delta\phi(t_k)] >|$, where $sign$ represents signum function, $<>$ stands for mean and Φ is a phase difference between two iEEG signals. For calculation of instantaneous phase see the phase-amplitude coupling paragraph. PLI was calculated in 1 second non-overlapping intervals with time-lag. Maximum time-lag was equal to $f_{max}/2$ of selected frequency band. The maximum value of PLI was stored with its time-lag value. Time-lag of maximum PLI value was evaluated as a separate feature.

2.7.10. Phase synchrony (bivariate feature)—Instantaneous phase of each signal was calculated the same way as in phase-amplitude coupling section. Phase synchrony (PS) was then calculated as $PS = \sqrt{[(<COS(\phi X_t)>)^2 + (<sin(\phi Y_t)>)^2]}$, where ΦX_t is instantaneous phase of signal X, ΦY_t is instantaneous phase of signal Y, $<>$ stands for mean and for square root.

2.7.11. Phase consistency (bivariate feature)—Calculation of phase consistency between two signals, regardless of any phase shift between signals. First, phase synchrony (PS, defined above) was calculated for multiple steps of time delay between two signals. Phase consistency (PC) was then calculated as *PC = <PS>·(1-std(PS)/0.5)*, where std is the standard deviation and $<>$ stands for mean.

2.8. Feature selection

Feature selection was carried out to determine the relevant features for classification (in both datasets separately and together for joined dataset). The features were separated into three groups: HFO features, univariate features and bivariate features (connectivity) to take into account different information they represent. Each group of features was evaluated separately by ANOVA. F-score values were used to determine the features that carry the most information for pathological tissue localization. The relevant features in each group were selected by determining outliers of F-score values using modified z-score with threshold set to 3 (Iglewicz and Hoaglin, 1993). Only features selected in respective dataset were used in SVM model for all patients in that dataset.

2.9. Support Vector Machine Classifier

Selected features were used to train and test an SVM model for classification of tissue under individual electrodes as normal or pathologic. Weights were applied to correct for the imbalanced dataset resulting from more non-pathological channels than the pathological ones. The weights were calculated as inversely proportional to class frequencies. Leave-one-patient-out cross validation was used to train and test the SVM. In each iteration, the data of one patient was held out for testing while the SVM was trained on the remaining data. To obtain the best possible performance, both linear and radial basis function (RBF) kernels were tested and a parameter sweep was carried out to determine the optimal value of the penalty parameter C and gamma parameters. The best performing parameters were used for final classification (Table 2). To evaluate the performance of the SVM models, the probability estimate of correct target classification was used to create receiver operating curves (ROC) and area under the curves (AUC) for each leave-one-out iteration.

2.10. Model evaluation

To evaluate the feasibility of SVM for different usage scenarios the feature selection and subsequent SVM model training were done for three definitions of pathological tissue: **1) Seizure onset zone**, as a standard definition of pathological tissue commonly defined in clinical practice. **2) Resected tissue,** in patients with excellent post-surgical outcome (ILAE 1 & Engel 1). **3) Resected tissue overlapped with SOZ** in patients with excellent post-surgical outcome. This overlap was used to compensate for non-pathological tissue removed

as part of the surgical margin. For example, in patients that have a standard anterior temporal lobectomy approximately 3–4 cm of lateral temporal neocortex is resected (Wiebe et al., 2001), even if apparent pathology is confined to the mesial temporal structures. The trained SVM model was also used to classify pathological channels in patients with poor surgical outcome to assess if tissue under contacts classified as pathologic was not resected during the surgery. The evaluation was done on the whole dataset as well as separately on the datasets from two institutions. Testing for seizure onset zone, resected tissue, and resected tissue overlapped with SOZ in Mayo Clinic, Brno center and both datasets together resulted in 9 runs of the algorithm. Statistical significance of the average AUCs was tested with a Hanley-McNeil test by comparing them to chance (AUC=0.5).

To evaluate the clinical relevance of the SVM model for individual patients, model training and classification were performed on resected tissue overlapped with SOZ in excellent outcome patients in a leave-one-out fashion. The classification of contacts in poor outcome patients was done by a model trained on all excellent outcome patients. To eliminate contacts misclassified due to residual noise the contacts classified as pathologic were clustered based on their spatial distribution in MNI space with the nearest neighbor clustering algorithm were radius was set to 2*shortest distance between contacts, i.e. 2 cm in patient space. Only the cluster with the highest mean probability of being pathologic was chosen (Figure 1). We defined true positive (TP) finding when all channels classified as pathological were within the resected area and patient had excellent outcome. False positive finding (FP) was defined when all channels classified as pathological were resected but the patient had poor surgical outcome. True negative (TN) finding was defined when at least one channel classified as pathological was outside the resected area and the patient had poor outcome. False negative (FN) finding was defined when at least one channel classified as pathological was outside the resected area and the patient had an excellent outcome. Negative predictive value (NPV) defined as TN / (TN + FN) and positive predictive value (PPV) defined as TP / (TP + FP) were calculated.

3. Results

3.1. Feature selection

The best performing features for all targets and both institutions are summarized in Table 3. Relative entropy was the most selected feature especially above the alpha (8–12 Hz) frequency range. Relative entropy in the low gamma (20–45 Hz) and ripple (80–250Hz) bands were selected in all runs of the algorithm. Oscillatory events detected by the line-length algorithm were the second most selected feature from alpha (8–12 Hz) band to ripple band (80–250Hz). Fast ripple HFO detected by CS algorithm (Cimbálník et al., 2018) was selected in 6 runs of the algorithm. Figure 2 shows distributions of two best performing features in Brno center dataset.

Notably, oscillatory event features were more often selected in runs using the Brno center dataset, whereas in runs with Mayo Clinic dataset the connectivity features were selected.

3.2. Pathologic tissue localization

The performance of the algorithm was evaluated for three different classifications of pathologic tissue (SOZ contacts; resected contacts; and SOZ overlapped with resected contacts) in both dataset separately as well as combined dataset from both centers. All runs of the algorithm showed AUCs significantly better than chance (p < 0.001). The lowest AUCs were obtained for classification of SOZ targets 0.770, 0.770, 0.745 for Brno center and Mayo Clinic and combined datasets. Classification of channels over the resected tissue in excellent outcome patients showed better performance than classification of SOZ channels for the Brno center dataset (0.842) and combined datasets (0.747) but worse performance for Mayo dataset (0.729). Classification of channels in poor outcome patients showed decreased performance in all datasets. Classification of SOZ contacts within resected area in excellent outcome patients had the best performance compared to the other targets (0.952, 0.803, 0.838). The classification performance was reduced in poor outcome patients (Figure 3). The ROC classification results are summarized in Table 1. In the subset of 28 patients where the contacts in SOZ overlapped with the resected contacts, the tissue under the iEEG electrodes, classified as epileptogenic, was removed in 17/18 excellent outcome patients and was not entirely resected in 8/10 poor outcome patients. Evaluation of the SVM models for individual cases showed NPV = 1.0 and PPV = 0.9 for Brno center dataset, NPV = 0.8 and PPV = 0.89 for Mayo dataset and NPV = 0.7 and PPV 0.83 for the whole dataset which included patients from both institutions, summarized in Table 4.

4. Discussion

This study reports a multi-feature, machine learning approach for classification of electrodes placed in epileptogenic tissue. It is the first study to our knowledge to combine conventional iEEG features and iEEG connectivity measures. Current inter-ictal methods have largely been focused on a single biomarker of epileptogenic zone, e.g. HFO rate (Worrell et al., 2012). To date, this has been insufficient for clinical practice (Jacobs et al., 2018).

The recent study by Varatharajah et al. (Varatharajah et al., 2018) shows that the combination of multiple biomarkers can outperform algorithms based on a single biomarker. However, this study did not assess connectivity measures. In our data, bivariate measures, especially the relative entropy, substantially contributed to the detector's performance.

From all calculated features the HFO rate and relative entropy were the most relevant for the epileptogenic zone distinction. The limitations of HFOs as a unique biomarker of epileptogenic brain are now widely appreciated and include distinguishing physiological (Buzsaki et al., 1992) and pathological (Matsumoto et al., 2013) HFOs and false positive detections (Bénar et al., 2010; Roehri et al., 2017). The CS detector efficiently eliminates false detections by phase correlation of bandpass filtered signal with a low pass filtered signal, which leads to clear distinction of true oscillations (Cimbálník et al., 2018). But even with optimal HFO detectors the ability to localize epileptogenic brain using HFOs alone is challenging. The current findings in iEEG connectivity studies suggest that changes of connectivity in epileptogenic tissue may be a clinically useful signature of ictogenesis and can substantially contribute to conventional methods for automatic localization of seizure generating tissue. Entropy has the ability to characterize signal randomness and spectral

richness. To our best knowledge, this is the first SEEG study to utilize relative entropy between signals from adjacent contacts on the depth electrodes as a measure of connectivity. Epileptogenic regions are known for a statistically higher rate of spectrally rich events, e.g., HFOs or epileptiform discharges, compared to healthy brain (Frauscher et al., 2017; Khoo et al., 2018). Therefore, the calculation of relative values of entropy between pathological and non-pathological areas makes this measure compelling in achieving the best possible score. In the Brno center and Mayo Clinic datasets, different features were selected as the most relevant (Table 3). This implies that there may be a dependence on the electrodes, reference signals, and acquisition system used. Studies with different datasets are needed to elucidate the impact of these variables on pathologic tissue localization. Further, it is well recognized that variability of vigilance levels can have impact on electrophysiological features for localization of epileptogenic tissue (Baud et al., 2018; Gliske et al., 2018). Rates of HFO and epileptiform discharges were shown to be the highest in non-rapid eye movement (NREM) sleep (Staba et al., 2004) which could further enhance the precision of the SVM model. Patients from Brno center were recorded during the day, whereas patients from Mayo Clinic were recorded at night. Therefore it is likely that differences between datasets and subsequent feature selection might also be caused by different states of vigilance. All of these variables had likely some influence on the presented results. Future studies with larger datasets should explore their impact on pathological tissue localization in more detail.

Pathological tissue classification by SVM models which combine HFO features with univariate and bivariate features show superior performance to algorithms utilizing these features or groups of features separately (Cimbalnik et al., 2018; Varatharajah et al., 2018). Classification of tissue under individual electrodes, which is the clinically relevant classification, was the most successful for the definition of SOZ contacts overlapped with resected area in excellent outcome patients. Using the trained SVM models on patients with poor surgical outcome resulted in worse AUC suggesting that channels identified by the algorithm as pathologic were not resected during surgery. Indeed, validating the SVM models using post-surgical outcome proved that resection of channels classified as pathologic led to excellent outcome while failure to resect these channels resulted in poor outcome. The presented algorithm showed similar performance on datasets from two institutions in different day times and clinical settings. Combining the datasets from both institutions resulted in worse performance both in ROC analysis and individual patient analysis which is likely due to difference in selected features.

The architecture of our approach and underlying software is modular, allowing to add other potentially useful features without the need to modify the whole data and model training pipelines. The modularity of the algorithm allows for easy utilization of other advanced processing pipelines (Fedele et al., 2017) or potential biomarkers of epileptogenicity such as very high-frequency oscillations (Brázdil et al., 2017), spike onset zone (Khoo et al., 2018), or low frequency activity (Vanhatalo et al., 2005). Further improvements in pathological tissue classification might be achieved by normalization of calculated features by the values found in normal human brain (Frauscher et al., 2018; Guragain et al., 2018). Recent studies have also reported that epileptogenic activity is changing over time, different states of vigilance and in different brain structures (Baud et al., 2018; Gliske et al., 2018; Guragain et al., 2018). Advanced iEEG signal processing methods might also be dependent on the length

of the analyzed segment (Fraschini et al., 2016). In this study, either resting-state or sleep recordings were analyzed, with a minimum length of 30 minutes without distinction of the states of vigilance or anatomical structure. Testing of the algorithm in specific sleep stages, resting-state conditions, different length of recording and specific anatomical structures can further improve its classification performance.

5. Limitations

Three definitions of pathological tissue used in this study are not optimal surrogate for pathological tissue definition. The definition of SOZ suffers from subjective visual determination by medical staff and the resection of such tissue does not guarantee seizure freedom (Téllez-Zenteno et al., 2010). Resected areas in excellent outcome patients often includes normal brain tissue in addition to electrophysiologically abnormal tissue. To overcome the problems of the former two definitions, we considered iEEG channels on a depth electrode pathological, if they were resected, and previously marked as SOZ. However, this definition is not guaranteed to encompass the whole pathological area of the epileptic brain. All of the definitions used suffer from substantial spatial undersampling of the brain tissue due to the limitations of clinical iEEG recordings (Stead et al., 2010; Worrell et al., 2012).

The presented method cannot be applied to multifocal patients due to spatial clustering, which was used to obtain the cluster of contacts with the highest probability of being pathologic. Nonetheless, this can likely be overcome in the clinical setting by visualization of all contact clusters and their probability (Figure 1) which could potentially be an invaluable tool for surgery planning. In addition, the referential signal was computed as average signal from contacts located in white matter which makes this method inapplicable to cases where white matter was not implanted.

Utilization of connectivity measures in a bivariate manner, i.e. calculation of relations between two adjacent contacts on one depth electrode, can introduce potential bias in final results. This is a well known limitation of bivariate measures in EEG signal processing, which is caused by ignoring possible relation with a third source.

The fact that no features were selected in the highest frequency band might reflect low signal-to-noise ratio in these frequencies. Conversely, absence of useful features in the lowest frequency bands could be caused by the short data segments used in this study. Further study of long-term recordings might reveal useful information in these bands.

Lastly, the use of this algorithm was limited to retrospective analysis of patients who had previously undergone surgery. Although the 'leave-one-out' approach can be interpreted as pseudo-prospective study, a true prospective study is required to clearly establish its effectiveness.

6. Conclusion

In this retrospective study in a modest number of patients, promising results were achieved in localization of epileptogenic regions by SVM models that combine multiple features from

30 minutes of inter-ictal iEEG recordings. Pilot testing of the proposed algorithm in two different datasets suggests it is suitable for further testing in prospective studies, and ultimately, its possible implementation in clinical practise. Our results also suggests better performance of multi-feature methods in epileptogenic tissue localization than methods, which are using single iEEG feature, e.g. HFO.

Supplementary Material

Refer to Web version on PubMed Central for supplementary material.

References

Antony AR, Alexopoulos AV, González-Martínez JA, Mosher JC, Jehi L, Burgess RC, et al. Functional connectivity estimated from intracranial EEG predicts surgical outcome in intractable temporal lobe epilepsy. PLoS One 20138(10):e77916. [PubMed: 24205027]

Baud MO, Kleen JK, Mirro EA, Andrechak JC, King-Stephens D, Chang EF, et al. Multi-day rhythms modulate seizure risk in epilepsy. Nat. Commun 20189(1). Available from: 10.1038/s41467-017-02577-y

Bénar CG, Chauvière L, Bartolomei F, Wendling F. Pitfalls of high-pass filtering for detecting epileptic oscillations: a technical note on "false" ripples. Clin. Neurophysiol 2010121(3):301–10. [PubMed: 19955019]

Bergey GK, Morrell MJ, Mizrahi EM, Goldman A, King-Stephens D, Nair D, et al. Long-term treatment with responsive brain stimulation in adults with refractory partial seizures. Neurology 201584(8):810–7. [PubMed: 25616485]

Bettus G, Wendling F, Guye M, Valton L, Régis J, Chauvel P, et al. Enhanced EEG functional connectivity in mesial temporal lobe epilepsy. Epilepsy Res 200881(1):58–68. [PubMed: 18547787]

Bragin A, Mody I, Wilson CL, Engel J Jr. Local generation of fast ripples in epileptic brain. J. Neurosci 200222(5):2012–21. [PubMed: 11880532]

Brázdil M, Cimbálník J, Roman R, Shaw DJ, Stead MM, Daniel P, et al. Impact of cognitive stimulation on ripples within human epileptic and non-epileptic hippocampus. BMC Neurosci 201516:47. [PubMed: 26205426]

Brázdil M, Pail M, Halámek J, Plešinger F, Cimbálník J, Roman R, et al. Very high-frequency oscillations: Novel biomarkers of the epileptogenic zone. Ann. Neurol 201782(2):299–310. [PubMed: 28779553]

Buzsaki G, Horvath Z, Urioste R, Hetke J, Wise K. High-frequency network oscillation in the hippocampus. Science 1992256(5059):1025–7. [PubMed: 1589772]

Cimbalnik J, Brinkmann B, Kremen V, Jurak P, Berry B, Van Gompel J, et al. Physiological and pathological high frequency oscillations in focal epilepsy. Ann Clin Transl Neurol 2018 Available from: 10.1002/acn3.618

Cimbálník J, Hewitt A, Worrell G, Stead M. The CS algorithm: A novel method for high frequency oscillation detection in EEG. J. Neurosci. Methods 2018293:6–16.

Cimbalnik J, Kucewicz MT, Worrell G. Interictal high-frequency oscillations in focal human epilepsy. Curr. Opin. Neurol 201629(2):175–81. [PubMed: 26953850]

Dauwels J, Eskandar E, Cash S. Localization of seizure onset area from intracranial non-seizure EEG by exploiting locally enhanced synchrony. Conf. Proc. IEEE Eng. Med. Biol. Soc. 20092009:2180–3.

Fedele T, Burnos S, Boran E, Krayenbühl N, Hilfiker P, Grunwald T, et al. Resection of high frequency oscillations predicts seizure outcome in the individual patient. Sci. Rep 20177(1):13836. [PubMed: 29062105]

Fisher RS, Velasco AL. Electrical brain stimulation for epilepsy. Nat. Rev. Neurol 201410(5):261–70. [PubMed: 24709892]

Fraschini M, Demuru M, Crobe A, Marrosu F, Stam CJ, Hillebrand A. The effect of epoch length on estimated EEG functional connectivity and brain network organisation. J. Neural Eng 201613(3): 036015.

Frauscher B, Bartolomei F, Kobayashi K, Cimbalnik J, van 't Klooster MA, Rampp S, et al. High-frequency oscillations: The state of clinical research. Epilepsia 201758(8):1316–29. [PubMed: 28666056]

Frauscher B, von Ellenrieder N, Zelmann R, Doležalová I, Minotti L, Olivier A, et al. Atlas of the normal intracranial electroencephalogram: neurophysiological awake activity in different cortical areas. Brain 2018141(4):1130–44. [PubMed: 29506200]

Gardner AB, Worrell GA, Marsh E, Dlugos D, Litt B. Human and automated detection of high-frequency oscillations in clinical intracranial EEG recordings. Clin. Neurophysiol 2007118(5): 1134–43. [PubMed: 17382583]

Gliske SV, Irwin ZT, Chestek C, Hegeman GL, Brinkmann B, Sagher O, et al. Variability in the location of high frequency oscillations during prolonged intracranial EEG recordings. Nat. Commun 20189(1):2155. [PubMed: 29858570]

Gnatkovsky V, de Curtis M, Pastori C, Cardinale F, Lo Russo G, Mai R, et al. Biomarkers of epileptogenic zone defined by quantified stereo-EEG analysis. Epilepsia 201455(2):296–305. [PubMed: 24417731]

Gross DW, Gotman J. Correlation of high-frequency oscillations with the sleep-wake cycle and cognitive activity in humans. Neuroscience 199994(4):1005–18. [PubMed: 10625043]

Guragain H, Cimbalnik J, Stead M, Groppe DM, Berry BM, Kremen V, et al. Spatial variation in high-frequency oscillation rates and amplitudes in intracranial EEG. Neurology 201890(8):e639–46. [PubMed: 29367441]

Iglewicz B, Hoaglin DC. How to Detect and Handle Outliers Asq Press; 1993.

Jacobs J, LeVan P, Chander R, Hall J, Dubeau F, Gotman J. Interictal high-frequency oscillations (80–500 Hz) are an indicator of seizure onset areas independent of spikes in the human epileptic brain. Epilepsia 200849(11):1893–907. [PubMed: 18479382]

Jacobs J, Wu JY, Perucca P, Zelmann R, Mader M, Dubeau F, et al. Removing high-frequency oscillations: A prospective multicenter study on seizure outcome. Neurology 2018 Available from: 10.1212/WNL.0000000000006158

Katzner S, Nauhaus I, Benucci A, Bonin V, Ringach DL, Carandini M. Local origin of field potentials in visual cortex. Neuron 200961(1):35–41. [PubMed: 19146811]

Kelly KM, Chung SS. Surgical treatment for refractory epilepsy: review of patient evaluation and surgical options. Epilepsy Res. Treat 20112011:303624. [PubMed: 22937231]

Khadjevand F, Cimbalnik J, Worrell GA. Progress and Remaining Challenges in the Application of High Frequency Oscillations as Biomarkers of Epileptic Brain. Curr Opin Biomed Eng 20174:87–96.

Khoo HM, von Ellenrieder N, Zazubovits N, He D, Dubeau F, Gotman J. The spike onset zone: The region where epileptic spikes start and from where they propagate. Neurology 201891(7):e666–74. [PubMed: 30006411]

Klimes P, Duque JJ, Brinkmann B, Van Gompel J, Stead M, St Louis EK, et al. The functional organization of human epileptic hippocampus. J. Neurophysiol 2016115(6):3140–5. [PubMed: 27030735]

Kremen V, Duque JJ, Brinkmann BH, Berry BM, Kucewicz MT, Khadjevand F, et al. Behavioral state classification in epileptic brain using intracranial electrophysiology. J. Neural Eng 201714(2): 026001.

Kucewicz MT, Cimbalnik J, Matsumoto JY, Brinkmann BH, Bower MR, Vasoli V, et al. High frequency oscillations are associated with cognitive processing in human recognition memory. Brain 2014137:2231–44. [PubMed: 24919972]

Leonardi M, Ustun TB. The global burden of epilepsy. Epilepsia 200243 Suppl 6:21–5.

Lüders H, Comair YG. Epilepsy Surgery Lippincott Williams & Wilkins; 2001.

Matsumoto A, Brinkmann BH, Matthew Stead S, Matsumoto J, Kucewicz MT, Marsh WR, et al. Pathological and physiological high-frequency oscillations in focal human epilepsy. J. Neurophysiol 2013110(8):1958–64. [PubMed: 23926038]

Nejedly P, Cimbalnik J, Klimes P, Plesinger F, Halamek J, Kremen V, et al. Intracerebral EEG Artifact Identification Using Convolutional Neural Networks. Neuroinformatics 2018 Available from: 10.1007/s12021-018-9397-6

Pearce A, Wulsin D, Blanco JA, Krieger A, Litt B, Stacey WC. Temporal changes of neocortical high-frequency oscillations in epilepsy. J. Neurophysiol 2013110(5):1167–79. [PubMed: 23761699]

Roehri N, Pizzo F, Bartolomei F, Wendling F, Bénar C-G. What are the assets and weaknesses of HFO detectors? A benchmark framework based on realistic simulations. PLoS One 201712(4):e0174702. [PubMed: 28406919]

Staba RJ, Wilson CL, Bragin A, Fried I, Engel J Jr. Sleep states differentiate single neuron activity recorded from human epileptic hippocampus, entorhinal cortex, and subiculum. J. Neurosci 200222(13):5694–704. [PubMed: 12097521]

Staba RJ, Wilson CL, Bragin A, Jhung D, Fried I, Engel J Jr. High-frequency oscillations recorded in human medial temporal lobe during sleep. Ann. Neurol 200456(1):108–15. [PubMed: 15236407]

Stam CJ, Nolte G, Daffertshofer A. Phase lag index: assessment of functional connectivity from multi channel EEG and MEG with diminished bias from common sources. Hum. Brain Mapp 200728(11):1178–93. [PubMed: 17266107]

Stead M, Bower M, Brinkmann BH, Lee K, Marsh WR, Meyer FB, et al. Microseizures and the spatiotemporal scales of human partial epilepsy. Brain 2010133(9):2789–97. [PubMed: 20685804]

Téllez-Zenteno JF, Ronquillo LH, Moien-Afshari F, Wiebe S. Surgical outcomes in lesional and non-lesional epilepsy: A systematic review and meta-analysis. Epilepsy Res 201089(2–3):310–8. [PubMed: 20227852]

Tzourio-Mazoyer N, Landeau B, Papathanassiou D, Crivello F, Etard O, Delcroix N, et al. Automated anatomical labeling of activations in SPM using a macroscopic anatomical parcellation of the MNI MRI single-subject brain. Neuroimage 200215(1):273–89. [PubMed: 11771995]

Van Gompel JJ, Worrell GA, Bell ML, Patrick TA, Cascino GD, Raffel C, et al. Intracranial Electroencephalography with Subdural Grid Electrodes: Techniques, Complications, and Outcomes. Neurosurgery 200863(3):498–506. [PubMed: 18812961]

Vanhatalo S, Voipio J, Kaila K. Full-band EEG (FbEEG): an emerging standard in electroencephalography. Clin. Neurophysiol 2005116(1):1–8. [PubMed: 15589176]

Varatharajah Y, Berry B, Cimbalnik J, Kremen V, Van Gompel J, Stead M, et al. Integrating artificial intelligence with real-time intracranial EEG monitoring to automate interictal identification of seizure onset zones in focal epilepsy. J. Neural Eng 201815(4):046035.

Warren CP, Hu S, Stead M, Brinkmann BH, Bower MR, Worrell GA. Synchrony in normal and focal epileptic brain: the seizure onset zone is functionally disconnected. J. Neurophysiol 2010104(6): 3530–9. [PubMed: 20926610]

Wiebe S, Blume WT, Girvin JP, Eliasziw M, Effectiveness and Efficiency of Surgery for Temporal Lobe Epilepsy Study Group. A randomized, controlled trial of surgery for temporal-lobe epilepsy. N. Engl. J. Med 2001345(5):311–8. [PubMed: 11484687]

Worrell GA, Gardner AB, Stead SM, Hu S, Goerss S, Cascino GJ, et al. High-frequency oscillations in human temporal lobe: simultaneous microwire and clinical macroelectrode recordings. Brain 2008131:928–37. [PubMed: 18263625]

Worrell GA, Jerbi K, Kobayashi K, Lina JM, Zelmann R, Van Quyen ML. Recording and analysis techniques for high-frequency oscillations. Prog. Neurobiol 201298(3):265–78. [PubMed: 22420981]

Highlights

- Multi-feature approach in localization of epileptogenic tissue is superior to using single feature.

- Multi-feature approach can improve epileptogenic brain localization.

- The presented algorithm performed well on datasets from different institutions.

Significance

In this study, promising results were achieved in localization of epileptogenic regions by SVM models that combine multiple features from 30 minutes of inter-ictal iEEG recordings.
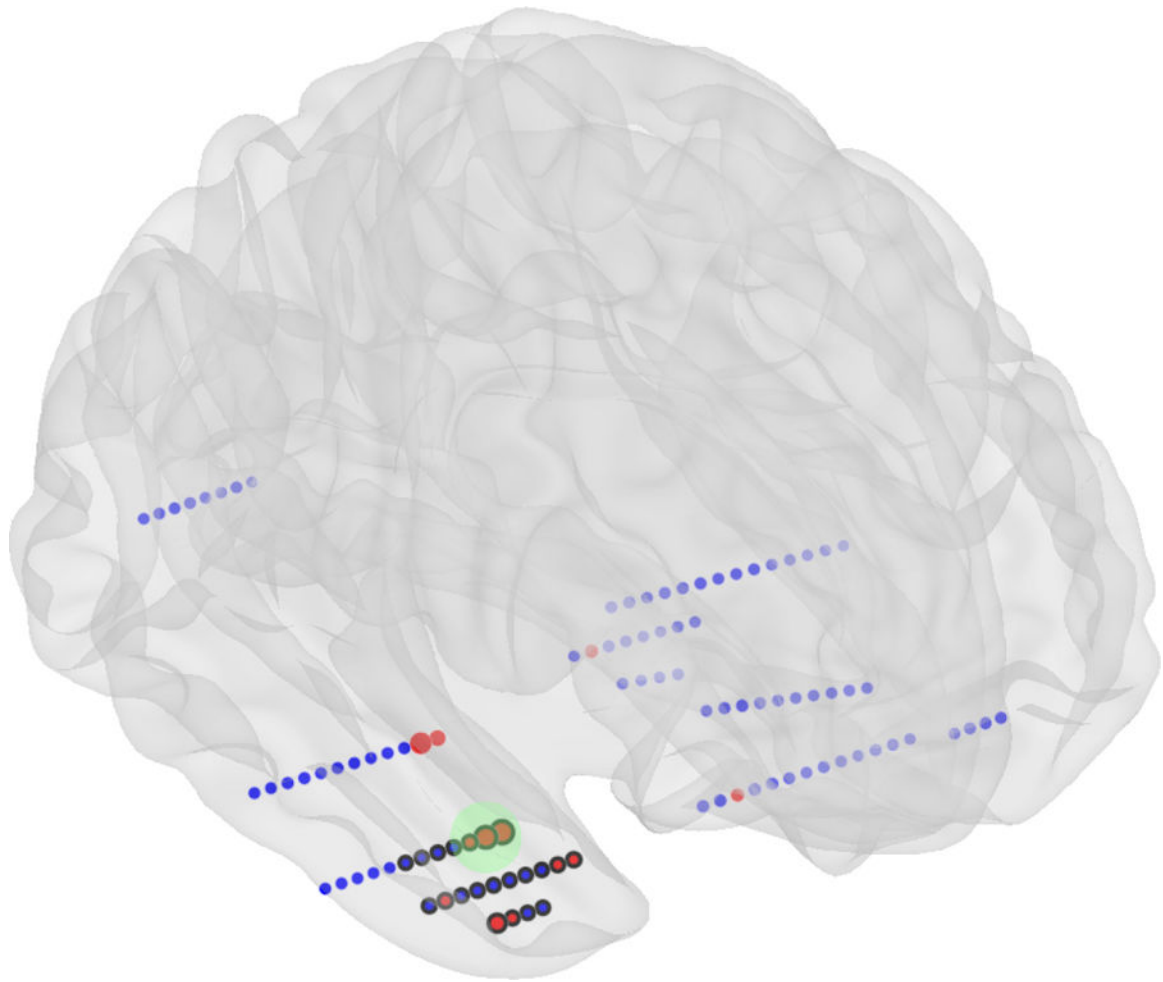
Figure 1.
Schematic illustration depth electrodes implanted in a brain. Localization of pathological tissue example. Red disks represent the channels identified by the SVM as pathological. The cluster (green circle) with the highest mean probability is selected as the final localization. Channels with black border were localized in the resected tissue.
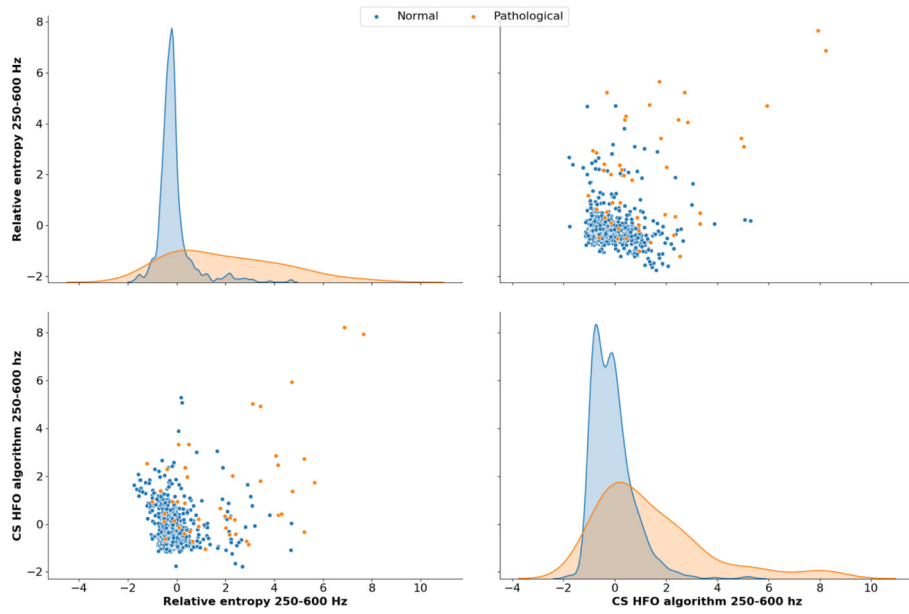
Figure 2.
Two best performing features in Brno dataset with SOZ ∩ resected area target. Relative entropy in FR frequency band and FR HFO show the highest association with the pathology. Distributions of both features demonstrate a long tail.

Figure 3.
ROC curves for Brno dataset with SOZ ∩ resected area target. Grey lines represent classification of electrodes in individual patients during cross-validation iterations. Blue lines represent mean ROC curves. ROC analysis in poor outcome patients shows decreased performance indicating that some channels classified by the SVM model as pathologic were not resected.

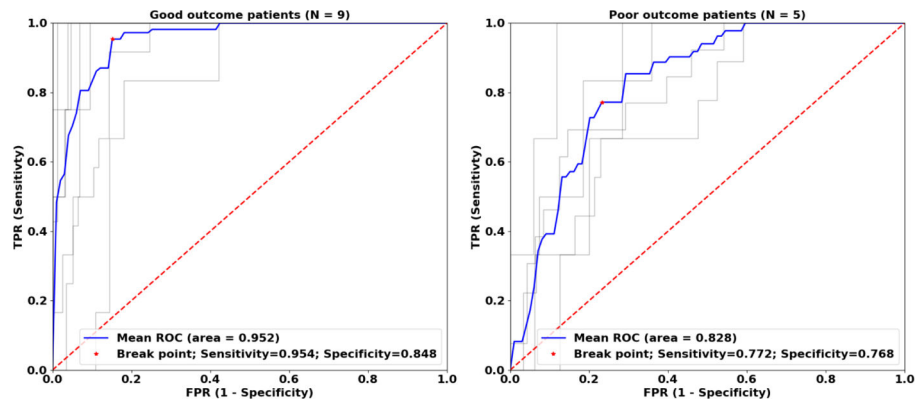**Table 1:**

The Receiver Operating Curve classification results for different datasets and different definition of epileptogenic tissue.

Target	SOZ	Resected		SOZ+Resected	
Outcome	All	Good	Bad	Good	Bad
Mayo	0.770(N=34)	0.729(N=9)	0.558(N=5)	0.803(N=9)	0.623(N=5)
Brno	0.770(N=43)	0.842(N=9)	0.776(N=7)	0.952(N=9)	0.827(N=5)
Joined	0.745(N=77)	0.747 (N=18)	0.560(N=12)	0.838(N=18)	0.592(N=10)

Table 2:

The best performing parameters for Support Vector Machine for different datasets and different definition of epileptogenic tissue.

Dataset	SOZ	Resected	SOZ+Resected
Mayo	rbf, C=0.1, gamma=0.001	rbf, C=10, gamma=0.001	rbf, C=10, gamma=0.001
Brno	rbf, C=10, gamma=0.001	rbf, C=0.1, gamma=0.01	linear, C=0.001
Joined	rbf, C=0.01, gamma=0.001	rbf, C=1, gamma=0.001	rbf, C=0.1, gamma=0.001

Table 3:

The best performing features.

Bands (Hz)	1–4			4–8			8–12			12–20			20–45			55–80			80–250			250–600			600–1000		
	B	M	J	B	M	J	B	M	J	B	M	J	B	M	J	B	M	J	B	M	J	B	M	J	B	M	J
HFO																											
Line Length					○◉		○◉	◉	○◉	○●◉	◉	●◉	●◉	◉	●◉		◉	◉	○◉		○◉					●	
CS detector																		○		○●◉			○◉	○◉			
Univariate																											
Power in band		●				●		◉	●	○◉	●		○◉				○										
Freq –amp coupling																											
Phase – ampcoupling								○																			
Power spectral entropy																											
Bivariate																											
Correlation		○			○															●◉			●				
Correlation with lag														●						●◉			●				
Correlation delay					◉			◉																			
Phase synchrony																				●◉			●				
Phase consistenc y																				●			●				
Phase lag index																				◉	●						
Phase pal index delay	○	●	●			●																	○◉	●			
Relative entropy					○	●		○◉	●◉	●	○●◉	○●◉	○●◉	○●◉	○●◉	○●◉	●	○●	●◉	○●◉	○●◉	○●◉	○●◉	○●◉	○●◉		

Seizure onset zone=○, Resected=●, Resected+SOZ=◉

B = Brno

M = Mayo

J = Joined

Table 4:

Evaluation of the Support Vector Machine models for individual cases.

Dataset	TP	FP	TN	FN	PPV	NPV	Sensitivity	Specificity
Mayo	8	1	4	1	0.89	0.80	0.89	0.80
Brno	9	1	4	0	0.90	1.00	1.00	0.80
Joined	15	3	7	3	0.83	0.70	0.83	0.70